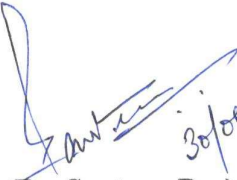


CERTIFICATE

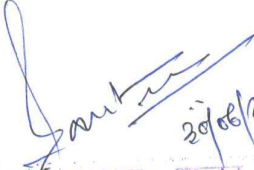
This is to certify that the thesis entitled “*Study of Graphene-based Metasurface Structures for Terahertz Frequency Applications*” being submitted by **Sambit Kumar Ghosh (Roll No-17091021)** to the Indian Institute of Technology (Banaras Hindu University) Varanasi, for the award of the Degree of Doctor of Philosophy in the Department of Electronics Engineering is a record of bonafide research work carried out absolutely by him under our supervision and guidance. The thesis has reached the standard; fulfilling the requirements of the regulations relating to the nature of the degree. The results embodied in this thesis have not been submitted to any other university or institute for the award of any degree or diploma.


(Dr. Somak Bhattacharyya) 30/6/22

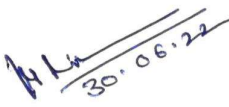
सहायक आचार्य/Assistant Professor
इलेक्ट्रॉनिकी अभियांत्रिकी विभाग
Department of Electronics Engineering
भारतीय प्रौद्योगिकी संस्थान
Indian Institute of Technology
(बनारस हिन्दू यूनिवर्सिटी)
(Banaras Hindu University)
वाराणसी/Varanasi-221005


(Dr. Santanu Das) 30/06/2022

Co-Supervisor


30/06/2022

Dr. SANTANU DAS/डा० शान्तनु दास
Assistant Professor/असिस्टेंट प्रोफेसर
Department of Ceramic Engg./सैरेमिक इंजिनियरिंग विभाग
Indian Institute of Technology (BHU)/भारतीय प्रौद्योगिकी संस्थान वी.एच.यू.
Varanasi-221005, U.P., India/वाराणसी-२२१००५, उ०प्र०, भारत


(Prof. V. N. Mishra) 30.06.22

Head of the Department

आचार्य व विभागाध्यक्ष / PROFESSOR & HEAD
इलेक्ट्रॉनिकी अभियांत्रिकी विभाग / Department of Electronics Engineering
भारतीय प्रौद्योगिकी संस्थान (का.हि.वि.) / Indian Institute of Technology (BHU)
वाराणसी / Varanasi-221005 (INDIA)

CANDIDATE'S DECLARATION

I, Sambit Kumar Ghosh, certify that the work embodied in this thesis is my own bonafide work and carried out by me under the supervision of Dr. Somak Bhattacharyya and co-supervision of Dr. Santanu Das from "25/07/2017" to "30/06/2022", at the Department of Electronics Engineering, Indian Institute of Technology (BHU), Varanasi. The matter embodied in this thesis has not been submitted for the award of any other degree/diploma. I declare that I have faithfully acknowledged and given credits to the research workers wherever their works have been cited in my work in this thesis. I further declare that I have not willfully copied any other's work, paragraphs, text, data, results, etc., reported in journals, books, magazines, reports, dissertations, theses, etc., or available at websites and have not included them in this thesis and have not cited as my own work.

Date: 30/06/2022

Place: IIT (BHU), VARANASI

Sambit Kumar Ghosh

Signature of the Student

Sambit Kumar Ghosh

CERTIFICATE BY THE SUPERVISOR

It is certified that the above statement made by the student is correct to the best of our knowledge.

S. Bhattacharyya 30/6/22
(Dr. Somak Bhattacharyya)

Supervisor

Department of Electronics Engineering
IIT (BHU), Varanasi

(Dr. Santanu Das)

Co-Supervisor

Department of Ceramic Engineering
IIT (BHU), Varanasi

सहायक आचार्य/Assistant Professor
इलेक्ट्रॉनिकी अभियांत्रिकी विभाग
Department of Electronics Engineering
भारतीय प्रौद्योगिकी संस्थान
Indian Institute of Technology
(बनारस हिन्दू यूनिवर्सिटी)
(Banaras Hindu University)
वाराणसी/Varanasi-221005

Signature of Head of Department

"SEAL OF THE DEPARTMENT"
आचार्य/विभागाध्यक्ष / PROFESSOR & HEAD

इलेक्ट्रॉनिकी अभियांत्रिकी विभाग/Department of Electronics Engineering
भारतीय प्रौद्योगिकी संस्थान (का.हि.वि.)/Indian Institute of Technology (BHU)
वाराणसी/Varanasi-221005 (INDIA)

Dr. SANTANU DAS/डॉ० शान्तनु दास

Assistant Professor/असिस्टेंट प्रोफेसर

Department of Ceramic Eng./सामग्री इंजिनियरिंग विभाग
Indian Institute of Technology (BHU)/भारतीय प्रौद्योगिकी संस्थान (का.हि.वि.)
Varanasi-221005, U.P., India/वाराणसी-२२१००५, उ०प्र०, भारत.

COPYRIGHT TRANSFER CERTIFICATE

Title of the Thesis: **Study of Graphene-based Metasurface Structures for Terahertz Frequency Applications**

Name of the Student: **Sambit Kumar Ghosh**

Copyright Transfer

The undersigned hereby assigns to the Indian Institute of Technology (Banaras Hindu University), Varanasi all rights under copyright that may exist in and for the above thesis submitted for the award of the Doctor of Philosophy.

Date: 30/06/2022

Place: IIT(BHU), VARANASI

Sambit Kumar Ghosh
Signature of the Student

Sambit Kumar Ghosh

Note: However, the author may reproduce or authorize others to reproduce material extracted verbatim from the thesis or derivative of the thesis for author's personal use provided that the source and the Institute's copyright notice are indicated.

Acknowledgment

This dissertation is the culmination of my Ph.D. experience, which was like climbing a mountain step by step while encountering encouragement, struggle, bitterness, frustration, and faith. It gives me immense pleasure to take this opportunity to offer my heartfelt appreciation to everyone who contributed to this thesis and assisted me along this incredible journey toward my Ph.D.

I would like to take the opportunity to convey my heartfelt appreciation to **Dr. Somak Bhattacharyya**, my Ph.D. supervisor and **Dr. Santanu Das**, my Ph.D. co-supervisor for accepting me as a student without hesitation and exposing me to a fascinating and exciting field of research. They have always been patient and encouraging while discussing new ideas, guiding me in the right direction. This research would not have been possible without their assistance.

I am extremely grateful to my research performance evaluation committee (RPEC) members Dr. Smrity Dwivedi of the Department of Electronics Engineering and Prof. Sandip Chatterjee of the Department of Physics whose suggestions and critical comments during my semester progress presentations really helped me to shape my thesis. I also thank Dr. M. Thottappan, and other faculty members for their kind cooperation and encouragement during this journey.

I must acknowledge Prof. K.P. Singh, Prof P. K Jain, Prof. S.P. Singh, Prof. R.U. Khan, Dr. Amit Singh, and Prof. M. K. Meshram for teaching interesting and informative subjects during my coursework period. That study done in the initial days of my Ph.D. helped a lot in refreshing the basics of electronics, which helped a lot in my research work.

My special thanks to my seniors Dr. Anshu Sharan Singh, Dr. Rajan Agrahari, Dr. Vineet Singh, Dr. Siva Venkateshwara Rao V., Dr. A. P. Singh, Dr. Vikram Kumar, Dr. Arjun Kumar,

Dr. Akash, Dr. Prabhakar Tripathi, Dr. R. K. Singh, Dr. M. A. Ansari, Dr. Sudhir Bhaskar for their friendly attitude and academic support.

I am very much thankful to my seniors and colleagues research scholars of the CRMT laboratory for their help and efforts to make the lab an enthusiastic place for research. My thanks go to Dr. Soumojit Shee, Mr. S. G. Yadav, Mr. V. V. Reddy, Mr. Nisheeth Upadhyay, Mr. V. Veera Babu, Mr. G. Venkatesh, Mr. Hemant Kumar, Mrs. Kirtika Singh, Miss Pratibha Verma, Mr. Sougata Chatterjee, Mrs. Madhavi Chandra, Mr. Vishal. I would like to share special thanks to my all-time partners Mr. Nilotpall, Mr. Diptiranjana Samantaray, Mr. Abhinav Pratap Singh, Mr. Sanjeevmani Yadav, Mr. Arun Kumar Saurabh, and Mr. Rishibrind Upadhyay with whom I have shared many a tensed moment as well as joyful moments with them and they always cared well for me.

My thanks and sincere appreciations also go to all staff members of the CRMT laboratory, especially to Mr. Rajesh Kr. Rai and Mr. Sanjay Kr. Vishwakarma for their kind co-operation. No words of appreciation could express my gratitude for my family, who have always been with me although they were miles away from me. My special thanks to my elder brothers Dr. Suman Ghosh, Dr. Amit Kumar Ghosh and my sister-in-law Mrs. Chandana Guha, Mrs. Swagata Mazumdar who always considered my research as a top priority and tried his best to make my life comfortable.

No words of appreciation could express my gratitude for my parents Shri. Rajkumar Ghosh and Mrs. Chandana Ghosh who always encouraged me to follow my dreams and have always advised me to be a good human being first. Whatever I am today is because of their unconditional love, care, guidance, encouragement, and moral support. To put in one line, they sacrifice their own lives to make our life.

Last per not least, I owe a debt of gratitude to Lord Vishwanath to sail the journey and make this possible by being with me all the time.

I seek pardon to those whose names unintentionally I have missed inspite of their immense support. I would like to thank all those who directly or indirectly helped me to bring this thesis to fruition.

Sambit Kumar Ghosh
Thank you 30/06/2021

Sambit Kumar Ghosh

*This thesis is dedicated to my
Parents*

| CONTENTS | | |
|---|---|------|
| <i>List of Figures</i> | | XIII |
| <i>List of Tables</i> | | XXI |
| <i>List of Abbreviations</i> | | XXII |
| <i>List of Symbols</i> | | XXIV |
| Chapter 1: Introduction and Literature Review | | |
| 1.1 | Introduction | 1 |
| 1.2 | Mathematical Representation of Graphene | 4 |
| 1.3 | Properties of Graphene | 7 |
| 1.4 | Metasurface, Graphene-based Metasurface and Subsequent Developments | 17 |
| 1.5 | Motivation | 26 |
| 1.6 | Organization of Dissertation | 27 |
| Chapter 2: Tunable Graphene-Based Metasurfaces for Broadband Wave Absorption in Lower Mid-Infrared (MIR) Range & THz Gap | | |
| 2.1 | Introduction | 30 |
| 2.2 | Design and Simulation of Structure | 34 |
| 2.3 | Simulated Results and Discussions | 37 |
| 2.4 | Design and Simulation of Structure | 47 |
| 2.5 | Design Evolution of the Structure | 52 |
| 2.6 | Simulated Results and Discussions | 54 |

| | | |
|--|---|-----|
| 2.7 | Conclusions | 62 |
| Chapter 3: Graphene-Based Metasurface for Tunable Absorption and Transmission Characteristics in the Near Mid-Infrared Region | | |
| 3.1 | Introduction | 64 |
| 3.2 | Design and Electromagnetic Execution of the Structure | 66 |
| 3.3 | Validation of the Simulated Results | 71 |
| 3.4 | Simulated Outputs and Explanations | 75 |
| 3.5 | Conclusions | 90 |
| Chapter 4: Terahertz Wave Conversion from Linear to Circular Polarization by Graphene Metasurfaces Featuring Tunable Performances | | |
| 4.1 | Introduction | 91 |
| 4.2 | Design and Simulated Outcomes | 92 |
| 4.3 | Validation of Simulated Outcomes Using Circuit | 100 |
| 4.4 | Ultrawideband Tunability Achieved by the RLCPC | 105 |
| 4.5 | Theory of Transmittive Polarization of EM Wave | 110 |
| 4.6 | Design of the Device | 112 |
| 4.7 | Simulated Results | 116 |
| 4.8 | Discussions | 120 |
| 4.9 | Conclusions | 129 |
| | | |

| | | |
|---|---|-----|
| Chapter 5: Graphene-based dual functional metadvice in the THz Gap | | |
| 5.1 | Introduction | 131 |
| 5.2 | Configuration and Working Principle of the Device | 133 |
| 5.3 | Simulated Results and Discussions | 135 |
| 5.4 | Circuit Realization | 144 |
| 5.5 | Discussions | 149 |
| 5.6 | Conclusions | 151 |
| Chapter 6: Conclusions and Future Scope | | |
| 6.1 | Conclusions | 153 |
| 6.2 | Suggestions for future scope | 158 |
| Publications | | 159 |
| References | | 126 |

| | | |
|------------------------|---|---|
| LIST OF FIGURES | | |
| Fig. 1.1: | Schematic representation of formation of covalent bonds in graphene surface. | 1 |
| Fig. 1.2: | Schematic representation of the (a). different physical forms of carbon and (b). formation of the allotropes. | 2 |
| Fig. 1.3: | Current applications of graphene and graphene derivatives. | 3 |

| | | |
|-------------------|---|----|
| Fig. 1.4: | Interband and intraband transitions induced by wave in doped graphene. | 8 |
| Fig. 1.5: | Schematic representation of the formation of SPP at (a) a dielectric-metal interface and (b) interfaces between dielectric-metal-dielectric structures. | 12 |
| Fig. 1.6: | Schematic representation of the formation of SPP at the dielectric-metal interface. | 13 |
| Fig. 1.7: | Schematic representation of the formation of LSPR around the metallic nanoparticles smaller than the incident wavelength. | 14 |
| Fig. 1.8: | Schematic representation of metasurface structures. | 17 |
| Fig. 1.9: | (a). Metallic metasurface structure for electromagnetic wave absorption and (b). dual-band absorptivity response under normal incidence and (c). single band absorptivity response under 90° polarization angle. | 18 |
| Fig. 1.10: | (a, b). Metallic metasurface structure for triple-band electromagnetic wave absorption and (c, d) fabricated prototype and (e). comparison of the simulated and measurement results. | 19 |
| Fig. 1.11: | Metallic frequency selective structure integrated with lumped components to produce absorption along with a transmission band. | 20 |
| Fig. 1.12: | (a, b). Multilayer metasurface structure for the cross-polarization manipulation of the electromagnetic wave and (c, d). Comparison of the co- and cross-polarized reflection coefficients extracted from HFSS and measurement. | 20 |
| Fig. 1.13: | (a). Single layer metallic metasurface structure for the cross-polarization conversion of the EM wave and (b). comparison of the simulated and measured co- and cross-polarized reflection coefficients. | 21 |

| | | |
|-------------------|--|----|
| Fig. 1.14: | (a). Graphene metasurface structure for narrowband electromagnetic wave absorption and (b). absorptivity responses under the variation of the Fermi energy in graphene layer. | 22 |
| Fig. 1.15: | (a). Graphene multilayer metasurface structure for wideband electromagnetic wave absorption and (b). absorptivity responses under the variation of the thickness of the substrate. | 23 |
| Fig. 1.16: | Theory and experimental study of un-patterned bi-layer graphene. | 24 |
| Fig. 1.17: | (a). Multi-layer metal-graphene hybrid metasurface structure for the reflective circular-polarization conversion of the EM wave and (b). variations of the axial riation response under different Fermi energy values. | 25 |
| Fig. 2.1: | (a) Top view and (b) 3-D perspective view of the wideband graphene-based metasurface absorber in lower MIR region. | 34 |
| Fig. 2.2: | Frequency responses of (a) reflectivity of the designed absorber and (b) absorptivity. | 36 |
| Fig. 2.3: | Frequency responses of the parametric variations of (a) gap between symmetric elements (q) and (b) dimension of the square shaped graphene layer in the middle of the slotted area (c). | 38 |
| Fig. 2.4: | Variation of absorptivity (a) due to the change in substrate thickness (h) and (b) change in periodicity (a) of the unit cell. | 39 |
| Fig. 2.5: | Absorptivity variations under (a) overall size of graphene layer (b) along with (b) the thickness (d) of the principal arm of the symmetric graphene layer. | 40 |
| Fig. 2.6: | Responses of absorption bandwidth (a) under different relaxation time (τ) and (b) by applying different chemical potential (μ). | 41 |
| Fig. 2.7: | Responses of the wide absorption bandwidths under (a) different polarization angles (ϕ), and different incident angles (θ) for (b) TE polarization and (c) TM polarization. | 42 |
| Fig.2.8: | Frequency responses of (a) real values of ϵ_{eff} and μ_{eff} (b) imaginary values of ϵ_{eff} and μ_{eff} . | 42 |
| Fig. 2.9: | (a) Electric field distributions at (a) 4.21 THz, (b) 6.78 THz and (c) 9.27 THz. | 44 |
| Fig. 2.10: | (a) Surface current distributions for (a) top layer and (b) bottom layer of proposed metasurface structure at 4.21 THz, 6.78 THz and 9.27 THz. | 45 |

| | | |
|-------------------|---|----|
| Fig. 2.11: | Power loss on the graphene based metasurface at (a) 4.21 THz, (b) 6.78 THz and (c) 9.27 THz. | 45 |
| Fig. 2.12: | (a) Top view, (b) 3-D perspective and (c) back view of the wideband graphene-based metasurface absorber in lower MIR region ($a = 6.7 \mu\text{m}$, $b = 1.8 \mu\text{m}$, $d = 3.8 \mu\text{m}$, $c = 0.9 \mu\text{m}$, $e = 0.9 \mu\text{m}$, $i = 1.4 \mu\text{m}$, $q = 1.8 \mu\text{m}$). | 48 |
| Fig. 2.13: | Equivalent circuit model of the proposed absorber structure. | 49 |
| Fig. 2.14: | Frequency responses of (a) reflection coefficient (r) and (b) reflection and transmission (t) co-efficients and (b) absorptivity (A) of the absorber structure in Fig. 1. | 50 |
| Fig. 2.15: | Development of the final structure through different shapes of (a) only square, (b) square patch with optimized both arms, (c) square patch with optimized both arm's length upto periodicity, (d) only fractal (e) fractal with vertical arm (f) fractal with horizontal arm and (g) fractal with both arms. | 53 |
| Fig. 2.16: | Frequency responses of (a) different structural formations of top graphene layer keeping the bottom graphene layer shape constant and (b) the final structure with gold bottom layer in replacement of the continuous graphene layer. | 54 |
| Fig. 2.17: | Variations of absorptivity (a) for the variation of middle square graphene geometry (d) and (b) due to the change in substrate thickness (h) of the unit cell. | 55 |
| Fig. 2.18: | Variations of absorptivity under (a) width variation of plus geometry of graphene layer (q) along with (b) the relaxation time (τ) variation. | 56 |
| Fig. 2.19: | Variations of absorptivity under (a) different values of top layer chemical potential ($T\mu$) and (b) bottom layer chemical potential ($B\mu$). | 57 |
| Fig. 2.20: | (a) Configuration of the proposed structure with the biasing setup and (b) Comparison of reflection (r) coefficient of the structure with and without the biasing setup. | 57 |
| Fig. 2.21: | Absorptivity responses under different (a) polarization angles and different incident angles (θ) for (b) TE polarization and (c) TM polarization. | 58 |

| | | |
|-------------------|--|----|
| Fig. 2.22: | (a) Electric field distributions at (a) 3.25 THz, (b) 6.16 THz and (c) 9.53 THz. | 60 |
| Fig. 2.23: | Surface current distributions for (a) top layer and (b) bottom layer of proposed metasurface structure at 3.25 THz, 6.16 THz and 9.83 THz along with magnitude plot. | 61 |
| Fig. 3.1: | (a) Top view, (b) bottom view, (c) side view and (d) perspective view of the wideband graphene-based metasurface raserber in the lower MIR region. | 66 |
| Fig. 3.2: | Frequency responses of reflection coefficient (R), transmission coefficient (T) and absorption (A) of EM wave incident on the designed raserber. | 67 |
| Fig. 3.3: | Schematic of the equivalent circuit model for the proposed device. | 70 |
| Fig. 3.4: | Spectral responses of (a) reflection characteristic of the periodic square graphene patch-based absorber only, (b) transmission characteristic of the periodically-slotted bottom gold layer only, and (c) comparison of both reflection and transmission responses between EM-simulation and equivalent circuit modeling of the proposed graphene based raserber. | 72 |
| Fig. 3.5: | Equivalent circuit model for the proposed graphene based raserber. | 73 |
| Fig. 3.6: | Absorption and transmission behavior of the proposed design with the variation of graphene patch dimensions (gP). | 76 |
| Fig. 3.7: | Absorption and transmission behavior of the proposed design with the variation of substrate thickness (t). | 76 |
| Fig. 3.8: | Absorption and transmission behavior of the proposed design with the periodicity (p) variation. | 77 |
| Fig. 3.9: | Absorption and transmission behavior of the proposed design with the triangular slot-gap (d) variation. | 77 |
| Fig. 3.10: | Responses of the wide absorption bandwidths under different values of relaxation time (τ). | 78 |

| | | |
|-------------------|---|----|
| Fig. 3.11: | (a) Biasing set-up for the proposed raserber and (b) frequency responses of reflection (R), absorption (A) and transmission (T) coefficients of the designed raserber while considering biasing scheme. | 80 |
| Fig. 3.12: | (a). The absorption and transmission behavior of the proposed device under variable DC biasing and blown up in Fig. 12(b) and (c) for clear understanding. | 82 |
| Fig. 3.13: | Different configurations of the proposed device with (a) one PSBGL, (b) two PSBGLs, (c) three PSBGLs, and (d) four PSBGLs. | 83 |
| Fig. 3.14: | Transmission responses (T) of the proposed device under different configurations of the periodically slotted bottom gold layer (PSBGL). | 83 |
| Fig. 3.15: | Response of the proposed raserber as a function of polarization angles (ϕ) and frequency (THz) in TE polarization. | 84 |
| Fig. 3.16: | Response of the proposed raserber as a function of polarization angles (ϕ) and frequency (THz) in TM polarization. | 85 |
| Fig. 3.17: | Response of the proposed raserber as a function of different incident angles (θ) and frequency (THz) in TE polarization. | 85 |
| Fig. 3.18: | Response of the proposed raserber as a function of different incident angles (θ) and frequency (THz) in TM polarization. | 86 |
| Fig. 3.19: | Electric field distributions of the overall structure at different frequencies. | 86 |
| Fig. 3.20: | Surface current distributions of the top layer and the bottom layer at different frequencies. | 87 |
| Fig. 4.1: | (a) Top view, and (b) perspective view of the wideband graphene-based metasurface (RLCPC) for linear to circular polarization conversion in lower MIR region ($r_1 = 7 \mu\text{m}$, $r_2 = 1 \mu\text{m}$, $r_3 = 5 \mu\text{m}$, $r_4 = 2 \mu\text{m}$, $p = 12 \mu\text{m}$, $t = 12 \mu\text{m}$, $t_l = 1 \mu\text{m}$). | 93 |
| Fig. 4.2: | Incident vertically polarized EM wave (E_y) is decomposed into two components E_{yE_1} and E_{yE_2} . | 95 |

| | | |
|-------------------|--|-----|
| Fig. 4.3: | Co-polarized (R_{yy}) and cross-polarized (R_{xy}) reflection coefficients. | 96 |
| Fig. 4.4: | Spectral performances in terms of (a). axial ratio (AR) and (b) ellipticity (e) of the proposed RLCPC. | 97 |
| Fig. 4.5: | (a). Spectral responses of axial ratio (AR) with the effect of individual elliptical slot on the unit cell of the graphene metasurface, and (b). comparison of the spectral responses of axial ratio (AR) with periodically-slotted graphene layer and periodically-slotted gold layer on top surface of the proposed RLCPC. | 98 |
| Fig. 4.6. | (a). Schematic of the transmission line model for the proposed graphene-based RLCPC and (b). the circuit model representation for the transmission line schematic for the proposed RLCPC. | 101 |
| Fig. 4.7: | Similar co-polarized reflection coefficients (R_{yy}) extracted from the circuit model of the RLCPC, as compared to the EM simulated results. | 102 |
| Fig. 4.8: | (a)-(c). Wave-matter interaction on the slotted graphene layer placed on top of SiO ₂ substrate of the proposed RLCPC (Magneto-plasmonic case) at 3.98 THz, 4.98 THz and 5.68 THz, respectively. | 104 |
| Fig. 4.9: | (a)-(c). Surface current distributions of the proposed RLCPC at 3.98 THz, 4.98 THz and 5.68 THz, respectively. | 105 |
| Fig. 4.10: | A probable biasing scheme for the proposed RLCPC. | 106 |
| Fig. 4.11: | Variation of AR of the EM wave reflected from the proposed RLCPC under different chemical potential values (μ). | 106 |
| Fig. 4.12: | Variation of AR of the EM wave reflected from the proposed RLCPC under different polarization ellipses formed at different frequencies at the reflection end of the proposed RLCPC while varying the chemical potential (μ) induced by the variable biasing voltage V_{dc} . | 107 |
| Fig. 4.13: | Variation of AR of the EM wave reflected from the proposed RLCPC under different oblique incidences (θ) of EM wave. | 108 |

| | | |
|-------------------|--|-----|
| Fig. 4.14: | (a) Top view, (b) bottom view and (c) side views of the unit cell of the proposed graphene-based TTLCPC in terahertz gap ($l_1 = 14 \mu\text{m}$, $l_2 = 7 \mu\text{m}$, $w_1 = 1.3 \mu\text{m}$, $w_2 = 1.3 \mu\text{m}$, $p_2 = 10 \mu\text{m}$, $p_3 = 12 \mu\text{m}$, $t = 2 \mu\text{m}$, $t_l = 0.5 \mu\text{m}$). | 112 |
| Fig. 4.15: | (a) Top view, (b) bottom view and (c) perspective view of the proposed realizable graphene-based TTLCPC. | 113 |
| Fig. 4.16: | Geometry of the top surfaced square graphene patches | 114 |
| Fig. 4.17: | Equivalent circuit model of the unit cell of the proposed TTLCPC | 115 |
| Fig. 4.18: | Frequency responses of the proposed TTLCPC in terms of (a) transmission coefficients (T_x & T_y) and (b) phase difference between them (T_x & T_y). | 117 |
| Fig. 4.19: | Frequency response of the proposed TTLCPC in terms of Axial ratio (AR) under 3 dB at 5.72 THz, 13.49 THz and 18.90 THz respectively. | 118 |
| Fig. 4.20: | Frequency response of the proposed TTLCPC in terms of ellipticity (e) within the whole frequency band. | 118 |
| Fig. 4.21: | Frequency response of the proposed TTLCPC in terms of Axial ratio (AR) with periodic graphene patches and when graphene patches are replaced by gold patches. | 119 |
| Fig. 4.22: | The orientation of the incident and transmitted E -fields through the proposed TTLCPC. | 119 |
| Fig. 4.23: | Wave-structure interaction on the graphene layer placed on top of the SiO_2 substrate of the proposed TTLCPC at different plasmonic resonant frequencies. | 121 |
| Fig. 4.24: | Polarization ellipses formed at the transmitting end of the proposed TTLCPC at the above said three different frequencies (5.72 THz, 13.49 THz and 18.90 THz). | 122 |

| | | |
|-------------------|---|-----|
| Fig. 4.25: | Axial ratio performances of the proposed TTLCPC within the spectral range under (a). different graphene patch sizes (p_2), (b). the variation of the periodicity of the unit cell (p_3) and (c). the variation of the thickness of the substrate (t). | 123 |
| Fig. 4.26: | Axial ratio (dB) versus frequency performance of the proposed TTLCPC under different chemical potential (μ) values of the graphene layer. | 124 |
| Fig. 4.27: | Axial ratio (dB) variations at the individual frequency bands of the proposed TTLCPC under different chemical potential (μ) values of the graphene layer. | 124 |
| Fig. 4.28: | Axial ratio (dB) versus frequency performance of the proposed TTLCPC under different incident angles (θ) of the wave. | 125 |
| Fig. 4.29: | Frequency response of the proposed TTLCPC at 5.72 THz, 13.49 THz and 18.90 THz when both slots are present on the backside gold layer of the proposed TTLCPC. | 126 |
| Fig. 4.30: | Frequency response of the proposed TTLCPC at 18.94 THz when only smaller slot with first configuration is present on the backside gold layer. | 126 |
| Fig. 4.31: | Frequency response of the proposed TTLCPC at 18.93 THz when only smaller slot with second configuration is present on the backside gold layer. | 127 |
| Fig. 4.32: | Frequency response of the proposed TTLCPC when only larger slot is present on the backside gold layer (a) at 13.67 THz and (b) at 18.82 THz, respectively. | 127 |
| Fig. 4.33: | Frequency responses of the proposed TTLCPC when 90° clockwise rotated larger slot is present on the backside gold layer (a) at 13.67 THz and (b) at 18.82 THz, respectively. | 128 |
| Fig. 4.34: | Frequency responses of the proposed TTLCPC when both slots are present on the backside gold layer (a) at 5.72 THz (b) at 13.49 THz and (c) at 18.90 THz, respectively. | 128 |

| | | |
|------------------|--|-----|
| Fig. 5.1: | (a, b, c) Top view, (d) perspective and (e) side view of the graphene-based dual-functional metadvice for absorption and cross-polarization conversion in THz-gap ($r_1 = 17 \mu\text{m}$, $r_2 = 12.5 \mu\text{m}$, $r_{11} = 15 \mu\text{m}$, $r_{22} = 6 \mu\text{m}$, $p = 30 \mu\text{m}$, $w_5 = 0.5 \mu\text{m}$, $l_5 = 8 \mu\text{m}$, $t = 1 \mu\text{m}$, $t_l = 1 \mu\text{m}$, $t_g = 9 \mu\text{m}$). | 133 |
| Fig. 5.2: | Physical illustration of the biasing scheme of the proposed device with an external static electric field, ζ , applied between the patterned graphene surface and the bottom gold surface in periodic environment of the unit cell. | 134 |
| Fig. 5.3: | (a). Optimized absorptivity performance of the proposed graphene-based dual-functional metadvice has been achieved when externally applied static electric field, $\zeta = 8.52 \text{ V/nm}$ (Mode I) and (b). optimized PCR has been achieved at its maximum value when static electric field, $\zeta = 0.44 \text{ V/nm}$ (Mode II). | 136 |
| Fig. 5.4: | Variation of the absorptivity (Abs) and cross-polarization conversion ratio (PCR) due to the change of the (a) height of the patterned graphene patch (t_g) from the ground gold surface and (b) size of the spatial span of the graphene patch (p_g) in Mode I operation of the device. | 137 |
| Fig. 5.5: | Variation of the absorptivity (Abs) and cross-polarization conversion ratio (PCR) due to the change of the (a) length of the plus-shaped slots on graphene patch (l_5) and (b) width of the plus-shaped slots on graphene patch (w_5) in Mode I operation of the device. One can experience that the field-intensities are dense at the periodically arranged plus-shaped slot regions on the graphene surface while the metadvice is working in Mode I operation. | 138 |
| Fig. 5.6: | Variation of the absorptivity (Abs) and cross-polarization conversion ratio (PCR) due to the change in the (a) outer major radii of the metallic split rings (r_1) and (b) inner major radii of the metallic split rings (r_{11}) in Mode II operation of the device. | 139 |
| Fig. 5.7: | Variation of the absorptivity (Abs) and cross-polarization conversion ratio (PCR) due to the change in the (a) outer minor radii of the metallic split rings (r_2) (b) inner minor radii of the metallic split rings (r_{22}) in Mode II operation of the device. | 140 |

| | | |
|-------------------|---|-----|
| Fig. 5.8: | Variation of the absorptivity (Abs) and polarization conversion ratio (PCR) due to the change in gap between the metallic split rings (w_3) within the unit cell in Mode II operation of the device. | 142 |
| Fig. 5.9: | Variation of the absorptivity (Abs) and polarization conversion ratio (PCR) due to the change in the periodicity (p) of the unit cell in (a) Mode I and (b) Mode II, operation of the device, respectively. | 143 |
| Fig. 5.10 | Circuit schematics for the (a) absorber structure (Mode I), (b) an equivalent circuit model of the proposed metadvice working as an absorber and (c) the comparison of circuit model simulated response and EM simulated outcomes. | 145 |
| Fig. 5.11: | Circuit schematics for the (a) cross-polarization converter structure (Mode II), (b) an equivalent circuit model for the proposed metadvice working as a cross-polarization converter and (c) the comparison of circuit model simulation and the EM simulation responses. | 146 |
| Fig. 5.12: | (a) Field concentration on the unit cell of the proposed device under two different conditions in Mode I and Mode II at 3.8 THz (Magneto-plasmonic case). | 150 |
| Fig. 5.13: | Surface current distributions on both (a) top and (b) bottom surfaces under two different conditions in Mode I and Mode II at 3.8 THz. | 151 |

| LIST OF TABLES | | |
|-----------------------|--|-----|
| Table. 1.1: | Plasma frequency for metals | 11 |
| Table. 2.1: | Brief Description of Simulation Results | 35 |
| Table. 2.2: | Calculation of Constitutive Parameters | 43 |
| Table. 2.3: | Comparison with Existing Graphene Metasurface Absorbers | 46 |
| Table. 2.4: | Comparison with Existing Graphene Metasurface Absorbers | 59 |
| Table. 3.1: | RLC Circuit Components Values for the Proposed Rasorber | 73 |
| Table. 3.2: | Comparison with Existing Rasorber Structures | 89 |
| Table. 4.1: | Comparison with Existing Graphene-based Metasurface LP to CP Converter | 93 |
| Table. 4.2: | Optimized Values for the Circuit Components | 104 |
| Table. 4.3: | Materials/Metals Used in the Formation of the Device | 113 |
| Table. 4.4: | Comparison With Existing Graphene-Based LP to CP Converters | 129 |
| Table. 5.1: | Comparison With Existing Dual-Functional Metadevices | 132 |
| Table. 5.2: | Optimized Values of the Circuit Components | 149 |

LIST OF ABBREVIATIONS

| Abbreviation | Full Form |
|---------------------|--------------------------------------|
| EM | Electromagnetic |
| THz | Terahertz |
| TE | Transverse Electric |
| TM | Transverse Magnetic |
| CST | Computer Simulation Technology |
| ADS | Advanced Design Systems |
| MS | Metasurface |
| MTM | Metamaterial |
| 1D | One-Dimensional |
| 2D | Two-Dimensional |
| 3D | Three-Dimensional |
| EMC | Electromagnetic Compatibility |
| EBG | Electromagnetic Band Gap |
| FSS | Frequency Selective Surface |
| HIS | High Impedance Surface |
| PEC | Perfect Electric Conductor |
| PMC | Perfect Magnetic Conductor |
| SPPs | Surface Plasmon Polaritons |
| SPR | Surface Plasmon Resonances |
| LSPPs | Localized Surface Plasmon Polaritons |

| Abbreviation | Full Form |
|---------------------|---------------------------------------|
| DUT | Device Under Test |
| DMD | Dielectric-Metal-Dielectric |
| MDM | Metal-Dielectric-Metal |
| GSPs | Graphene Surface Plasmon Polaritons |
| FP | Fabry-Perot |
| CP | Circular Polarization |
| LP | Linear Polarization |
| PCR | Polarization Conversion Ratio |
| RCS | Radar Cross Section |
| Abs | Absorptivity |
| RLCPC | Reflective-type LP to CP Conversion |
| TTLPCPC | Transmittive-type LP to CP Conversion |
| DFD | Dual Functional Device |
| NIR | Near Infrared |
| MIR | Mid Infrared |
| FIR | Far Infrared |
| LHCP | Left-Handed Circular Polarization |
| RHCP | Right-Handed Circular Polarization |
| AR | Axial Ratio |
| FARBW | Fractional Axial Ratio Bandwidth |
| CVD | Chemical Vapour Deposition |
| FABW | Fractional Absorption Bandwidth |
| FTBW | Fractional Transmission Bandwidth |
| PTC | Peak Transmission Coefficient |

Abbreviation**Full Form**

| | |
|--------|--|
| FBO | Frequency Band of Operation |
| PSBGL | Periodically Slotted Bottom Gold Layer |
| FP-LWA | Fabry perot-leaky wave antenna |
| FIT | Finite Integration Technique |

LIST OF SYMBOLS

| Symbol | Details |
|--------------------|---|
| σ_g | Surface conductivity of graphene |
| μ | Chemical Potential of graphene |
| k_B | Boltzmann's constant |
| e | Charge of an electron |
| E_f | Fermi energy of graphene |
| ω | Angular frequency of the photon |
| T | Room temperature (300 K) |
| Γ | Scattering rate of the Dirac electrons |
| T | Relaxation time |
| h | Plank's constant |
| \hbar | Reduced Plank's constant |
| $f_d(\varepsilon)$ | Fermi dirac distribution function |
| $\hbar\omega$ | Energy of a photon |
| v_f | Fermi velocity of the electrons |
| t_g | Thickness of the graphene layer |
| E_o | DC electrostatic bias |
| V_g | DC gate voltage |
| C_{ox} | Gate capacitance |
| n_s | Concentration of the charge carriers |
| E_{bd} | Breakdown voltage of the dielectric substrate |

| Symbol | Details |
|------------------|---|
| ϵ_r | Effective permittivity |
| J | Surface conductivity of graphene |
| E | Electric field component |
| σ_{intra} | Intraband conductivity |
| σ_{inter} | Interband conductivity |
| eV | Electron-volt |
| N | Inclusive movement of the free electrons |
| P | Polarization density of the electrons |
| f_p | Plasma frequency |
| q_{spp} | Wave vector of the SPP mode |
| k_j | SPP wavenumber |
| ξ | Static electric field |
| ϕ | Polarization angle |
| θ | Angle of Incidence |
| ϵ_{eff} | Effective permittivity |
| μ_{eff} | Effective permeability |
| δ_g | Skin depth of graphene |
| D_n | Normalized component of the displacement vector |
| β | Wave propagation constant |
| ω_p | Plasma frequency |
| T_μ | Chemical potentials of the top layer graphene layer |
| B_μ | Chemical potentials of the top layer graphene layer |

| Symbol | Details |
|---------------|--|
| β^P | Phase constant of the surface plasmon mode |
| β^{LM} | Phase constant of the leaky plasmon mode |
| k_{LM} | Wavenumber corresponding to the leaky plasmon mode |
| α_{LM} | Attenuation constant of the leaky plasmon mode |
| σ_R | Resistive conductivity of graphene surface |
| σ_J | Reactive surface conductivity of graphene surface |
| η_o | Characteristic impedance of the vacuum |
| λ_g | Guided wavelength |
| Z_o | Free space impedance |